ENU induced mutations causing congenital cardiovascular anomalies

Qing Yu[1], Yuan Shen[1], Bishwanath Chatterjee[1], Brett H. Siegfried[1,2], Linda Leatherbury[1,3], Julie Rosenthal[1], John F. Lucas[4,5], Andy Wessels[4], Chris F. Spurney[1,3], Ying-Jie Wu[1], Margaret L. Kirby[6], Karen Svenson[7] and Cecilia W. Lo[1,*]

[1]Laboratory of Developmental Biology, National Heart Lung and Blood Institute, National Institutes of Health, Bethesda, MD 20892-8019, USA
[2]Department of Pediatrics, National Naval Medical Center, Uniformed Services University of the Health Sciences, Bethesda, MD 20814-5000, USA
[3]Pediatric Cardiology, Children's National Medical Center, Washington, DC 20010, USA
[4]Department of Anatomy and Cell Biology, Medical University of South Carolina, Charleston, SC 29425, USA
[5]Pediatric Cardiology, Medical University of South Carolina, Charleston, SC 29425, USA
[6]Department of Pediatrics, Duke University Medical Center, Durham, NC 27710, USA
[7]The Jackson Laboratory, Bar Harbor, ME 04609, USA
*Author for correspondence (e-mail: loc@nhlbi.nih.gov)

Accepted 20 October 2004

Development 131, 6211-6223
Published by The Company of Biologists 2004
doi:10.1242/dev.01543

Summary

We used non-invasive high frequency ultrasound to screen N-ethyl-N-nitrosourea mutagenized mouse fetuses for congenital cardiovascular anomalies. We ultrasound scanned 7546 mouse fetuses from 262 mutagenized families, and identified 124 families with cardiovascular defects. Represented were most of the major congenital cardiovascular anomalies seen clinically. The ENU-induced mutations in several families were mapped using polymorphic microsatellite DNA markers. One family with forelimb anomalies and ventricular septal defects, phenotypes similar to Holt-Oram syndrome, and one family with transposition of the great arteries and heart situs anomalies were mapped to different regions of mouse chromosome 4. A third mutation causing persistent truncus arteriosus and craniofacial defects, phenotypes reminiscent of DiGeorge syndrome, was mapped to mouse chromosome 2. We note that mouse chromosomes 4 and 2 do not contain *Tbx5* or *Tbx1*, genes previously linked to Holt-Oram and DiGeorge syndromes, respectively. In two other families, the ENU-induced mutation was identified – *Sema3C*^{L605P} was associated with persistent truncus arteriosus with interrupted aortic arch, and the *Gja1*^{W45X} connexin43 mutation caused conotruncal malformation and coronary aneurysms. Although our screen was designed as a recessive screen, a number of the mutations showed cardiovascular phenotypes in both heterozygote and homozygote animals. These studies show the efficacy of ENU mutagenesis and high-throughput ultrasound phenotyping in recovering mutations causing a wide spectrum of congenital heart defects. These ENU-induced mutations hold promise in yielding new insights into the genetic basis for human congenital heart disease.

Key words: Congenital heart defects, Cardiovascular anomalies, ENU mutagenesis, Mouse mutants, Ultrasound imaging

Introduction

Congenital heart disease is one of the most common birth defects in humans, affecting approximately 0.5 to 5% of live births (Hoffman, 1995; Rosenthal, 1998; Hoffman and Kaplan, 2002). Clinically, congenital heart defects often are sporadic, have incomplete penetrance and show variable phenotypes. These clinical findings suggest that congenital heart anomalies are the result of complex genetic interactions and, additionally, that they may involve interplay between genes and environment (Strauss, 1998). Nevertheless, there are a handful of single gene mutations encoding transcription factors shown to cause human congenital heart disease, among them are two associated with nonsyndromic human congenital heart disease – *NKX2.5* and *GATA4* (Schott et al., 1998; Garg et al., 2003). *NKX2.5* mutations are linked with cardiac septal defects and atrioventricular (AV) conduction block, whereas *GATA4* mutations are linked to cardiac septal defects. In addition, a number of mutations in genes encoding transcription factors have been identified for syndromic congenital heart disease, including in: *TFAP2*, which is linked with Char syndrome, characterized by patent ductus arteriosus (Satoda et al., 2000); *ZIC2*, which is associated with X-linked heterotaxy (Gebbia et al., 1997); *TBX1*, linked with DiGeorge syndrome, characterized by craniofacial dysmorphism, heart outflow anomalies and thymus hypoplasia (Yagi et al., 2003); and *TBX5*, which is associated with Holt-Oram syndrome, characterized by atrial/ventricular septation defects and forelimb anomalies (Basson et al., 1997; Li et al., 1997b). In addition, mutations in the transcription factor *SALL4* have been linked to Okihiro syndrome, a

congenital disorder similar to Holt-Oram syndrome (Kohlhase et al., 2002).

Besides mutations in transcription factors, mutations in *PTPN11*, encoding protein tyrosine phosphatase SHP-2, has been linked to Noonan and LEOPARDS syndromes (Taraglia et al., 2001), which are characterized by pulmonary stenosis, atrial septal defects, and early onset hypertrophic cardiomyopathy (Noonan) or conduction anomalies (LEOPARD). Linkage has also been established for mutations in 7-dehydrocholesterol reductase in Smith-Lemli-Opitz syndrome (for a review, see Jira et al., 2003), which is characterized by AV canal defects, together with microcephaly, cleft palate, postaxial polydactyly or syndactyly. Finally, mutations in *Jagged1*, a ligand in the Notch signaling pathway, has been shown to cause Alagille syndrome, which is characterized by pulmonary outflow and other cardiac defects, bile duct paucity and other anomalies (Li et al., 1997a; Oda et al., 1997). Except for Smith-Lemli-Opitz syndrome, these mutations are autosomal dominant. It is important to note that not all individuals exhibiting the various syndromic congenital cardiovascular malformations have mutations in the identified genes. Rather, evidence suggests these congenital heart diseases are genetically heterogeneous.

Given the many difficulties involved in tracking the genetic basis for congenital heart anomalies in human populations, the pursuit of mouse models has become an invaluable avenue of investigation. Using embryonic stem cell gene-targeting approaches, gene function can be investigated by generating mice in which the endogenous allele has been knocked out or replaced. Indeed some of the gene-targeted mouse lines generated exhibit phenotypes resembling those seen in human congenital heart disease. The involvement of *Tbx1* in DiGeorge syndrome was in fact first indicated by the analysis of *Tbx1* knockout mice (Lindsay et al., 2001; Merscher et al., 2001; Jerome and Papaioannou, 2001), and only later was confirmation obtained for *TBX1* mutations in patients with DiGeorge syndrome (Yagi et al., 2003). Overall, studies with transgenic and knockout mouse models show that mice can be used effectively to model human congenital heart disease, although in many instances, the identification of genes or mutations causing cardiovascular defects has been serendipitous.

In this study, we explored the use of N-ethyl-N-nitrosourea (ENU) mutagenesis as an alternative approach for identifying genes that may contribute to congenital heart defects. Chemical mutagenesis allows a genome wide scan for genes that may be important in heart development and disease. Typically, such mutagenesis is conducted in an inbred mouse strain such as C57BL6/J, and when mutations of interest are found, the mutant mice are interbred with a different inbred mouse strain, allowing the rapid mapping of mutations by tracking linkage of the mutant phenotype with polymorphic microsatellite DNA markers. ENU mutagenesis has been successfully employed for a variety of focused phenotypic screens in mice, such as for mutations that cause cataracts, behavioral or circadian rhythm perturbations, atherosclerosis, hypertension and obesity (Favor, 1986; Vitaterna et al., 1994; Pickard et al.,1995; Svenson et al., 2003). Of crucial importance to the success of such screens is access to an appropriate high-throughput phenotyping tool – in our case, one suitable for the detection of congenital cardiovascular anomalies in mouse fetuses. In this study, we showed the efficacy of an advanced clinical ultrasound system for non-invasive cardiovascular phenotyping of mouse fetuses.

Ultrasound is routinely used clinically for assessing human cardiovascular structure and function, and has been used to examine mouse fetuses (Gui et al., 1996; Huang et al., 1998b; Srinivasan et al., 1998; Zhou et al., 2002; Maki et al., 2002; Leatherbury et al., 2003). There are several advantages with ultrasound phenotyping. First, it is non-invasive, and thus fetuses can be examined in utero, allowing for horizontal studies over many days. Second, it provides assessments of both cardiovascular structure and function. Third, it is a high-throughput procedure, as a hundred or more fetuses can be screened in a day. For this prenatal fetal screen, we adopted a recessive breeding scheme, with the expectation that this would yield the most deleterious phenotypes. Overall, our studies showed that mouse mutations causing congenital heart disease can be efficiently recovered by high-throughput fetal ultrasound phenotyping. Such studies hold promise in yielding new insights into the genetic basis for human congenital heart disease.

Materials and methods

ENU mutagenesis and breeding of mutagenized mice

C57BL6/J males were injected with fractionated doses of ENU (80 mg/kg of body weight three times at weekly intervals) (Weber et al., 2000). After a period of 10 weeks for the recovery of fertility, the mutagenized G0 males were mated to C57BL6/J female mice. The resulting G1 males were again mated to C57BL6/J females to generate G2 females. Four G2 females were backcrossed to their G1 father, and the resulting pregnant G2 females carrying the G3 fetuses were subject to ultrasound scanning. Further information on the mutagenesis and breeding protocols can be found at http://pga.jax.org/protocols.html.

Ultrasound imaging and Doppler echocardiography

An Acuson Sequoia C256 ultrasound system with a 15 MHz L8 linear phased array transducer was used to scan pregnant female mice placed on a heating pad and anesthesized with isofluorane anesthesia (1.5% in medical air). ECG electrodes and a rectal probe continuously monitored the mother's heart rate (450-550 bpm) and body temperature (36-37°C), respectively. Hair was removed from the abdomen, and pre-warmed ultrasound gel was applied. Color flow and spectral Doppler imaging were obtained from embryonic day (E)12.5 to E19.5. From E14.5, M-mode and 2D images were obtained from the fetus using short axis views of the ventricles and great vessels, apical three/four/five chamber views, and long axis views of the left ventricle, aorta and pulmonary arteries.

Necropsy and histology

Stillborn pups or pups that died within a day of birth were retrieved and fixed in 10% buffered formalin. Necropsy was performed to examine the heart, great vessels and aortic arch arteries. For histology, the heart and surrounding vessels were paraffin-wax embedded, sectioned, and stained with Hematoxylin and Eosin. Some were processed and examined by episcopic fluorescence image capture (Weninger and Mohun, 2002). Pups with apparent skeletal anomalies were further processed for Alizaren Red and Alcian Blue staining.

Genome scan analysis

To examine heritability and facilitate mapping of the mutation, G2 carrier females were intercrossed with C3H mice to generate C3H/C57BL6 hybrid offspring. These were then further intercrossed for cardiovascular phenotyping by echocardiography, followed by analysis via necropsy and histopathology. DNA collected from the

affected fetuses was PCR amplified using primers for 48 C3H/C57BL6 polymorphic microsatellite markers. The resultant PCR products were pooled and separated by capillary electrophoresis on the Avant 3100 Genetic Analyzer (Applied Biosystems), and the data generated were analyzed using the method of Neuhaus and Beier for recombinant interval haplotype analysis (Neuhaus and Beier, 1998). Thus, DNA markers located near the ends of each mouse chromosome are used to demarcate intervals that are treated as haplotypes for the purpose of linkage analysis. For the larger chromosomes (1, 2, 3, 4, 6), one or two additional markers are included to provide one or two additional intervals (proximal, middle, distal; see Table 2). The frequency with which recombinant haplotypes are found across the entire genome in the affected fetuses is tracked. The ENU-induced mutation is expected to lie in a chromosome interval that is consistently homozygous B6 in most or all of the affected fetuses, i.e. non-recombinant for C3H markers (corresponding to a 0 or 1 in Table 2).

Results

Non-invasive in utero Doppler echocardiography was used to examine G3 fetuses carried by pregnant G2 mothers backcrossed to their G1 fathers, with all of the offspring of each G1 male defined as a family. Most fetuses were scanned on two or three different days between E12.5 and E19.5. To track growth and development, the fetal crown to rump length, fetus area and heart area were measured using 2D ultrasound images (Fig. 1A). Cardiovascular structure and function were evaluated using a combination of 2D imaging, color flow/spectral Doppler analysis and M-mode imaging (Fig. 1). Cardiac function was assessed by measuring the shortening fraction using M-mode analysis, and by monitoring the fractional area change via 2D imaging.

Ultrasound scanning of 7546 G3 fetuses in 902 G2 mothers derived from 262 families yielded 495 fetuses with developmental anomalies. These were broadly categorized as prenatal lethal, growth retarded, and/or with cardiovascular defects. These gross classifications are overlapping, as fetuses that died prenatally often were also growth retarded and/or exhibited cardiovascular defects. Prenatal lethality was diagnosed by 2D imaging and Doppler interrogations, and corresponded to conceptuses with no heartbeat. Of the 495 abnormal fetuses, 188 (38%) from 91 (35%) families died prenatally. Growth retardation, defined as fetuses exhibiting crown to rump length and fetal area measurements two standard deviations below the mean, was observed in 106 fetuses (21%) from 67 (26%) families, whereas cardiovascular defects were observed in 339 fetuses (68%) from 124 (47%) families.

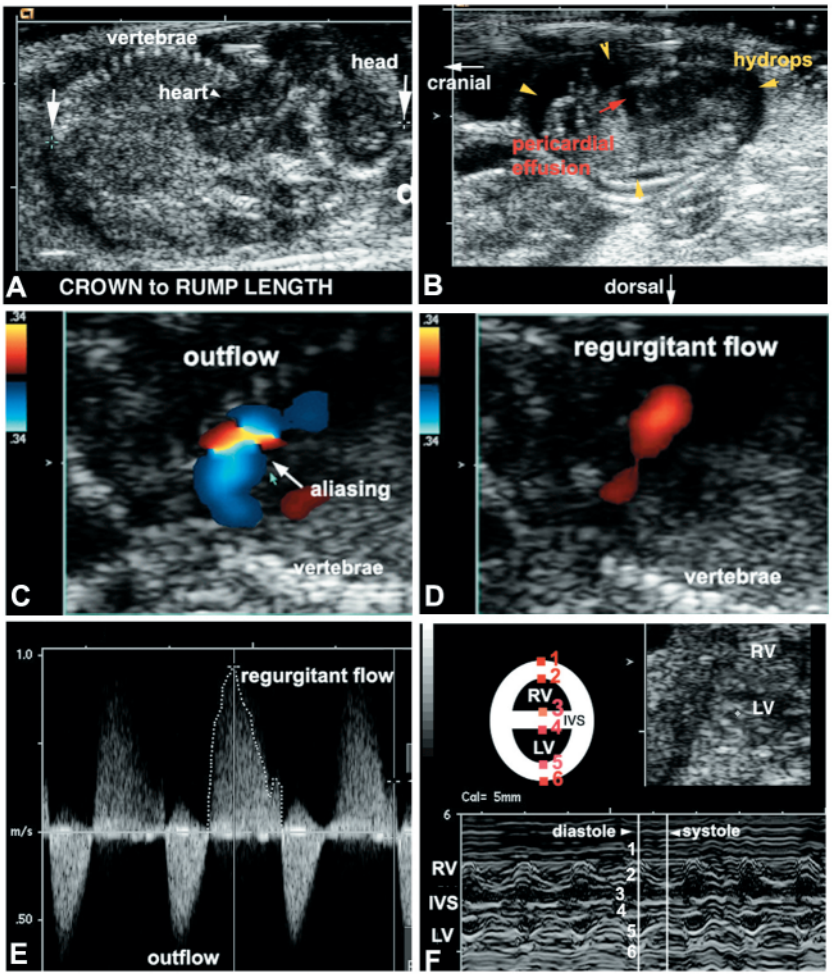

Fig. 1. Mouse fetal ultrasound imaging. (A) In utero 2D-ultrasound image of a fetus, showing two white arrows used to measure the crown to rump length. (B) A fetus showing pericardial effusion (red arrow) and hydrops (yellow arrows). (C,D) Color flow Doppler analysis showed outflow regurgitation in an E18.5 fetus. Aliasing (see arrow) associated with the outflow (C) indicated increased velocity. Superimposed on the outflow is a regurgitant diastolic flow (D). (E) Spectral Doppler analysis revealed an abnormal regurgitant flow. (F) M-mode images from an E17.5 fetus, obtained from a short axis view (see diagram), show the position of the right (RV) and left (LV) ventricular walls and the interventricular septum (IVS) through multiple cardiac cycles. Wall thickness, and chamber volume in diastole and systole can be obtained by measuring the distances between numbered positions (red color dots versus corresponding position in M-mode image).

Cardiovascular anomalies detected by ultrasound

The cardiovascular anomalies that could be detected by prenatal fetal ultrasound included arrhythmias, outflow regurgitations, increased outflow velocity, heart failure, hypertrophy and ectopia cordis (Table 1; see below). Arrhythmia was easily observed by spectral Doppler analysis and included premature systole, pause, bradycardia and tachycardia. However, bradycardia accounted for nearly half (42%) of the arrhythmias, which frequently is a manifestation of dying fetuses. Consistent with this, we note that 18% of fetuses with heart failure also exhibited bradycardia. Heart failure was discerned by dynamic 2D imaging, and is characterized by poor contractile function, pericardial effusion and hydrops (Fig. 1B). Contractile motion of the beating heart was assessed qualitatively using 2D video sequences, and quantitatively with measurements of ejection fraction,

Table 1. Fetal ultrasound screening for cardiovascular anomalies

	Families*	Necropsy/histology confirmed†	Mutant fetuses‡	Multiple echo scans§	Growth retarded¶	Prenatallethal¶	Bradycardia¶
All cardiovascular defects	124	–	339	–	81 (24%)	17 (5.0%)	–
Arrhythmia	67 (54%)	–	106 (31%)	23 (22%)	11 (10%)	10 (9.4%)	44 (42%)
Outflow regurgitation	43 (35%)	22 (51%)	93 (27%)	50 (54%)	44 (47%)	13 (14%)	20 (22%)
Outflow velocity increase**	30 (24%)	5 (17%)	37 (11%)	10 (27%)	9 (24%)	4 (11%)	2 (5.4%)
Heart failure	58 (47%)	42 (72%)	111 (33%)	26 (23%)	67 (60%)	16 (14%)	20 (18%)
Hypertrophy	44 (35%)	17 (39%)	77 (23%)	18 (23%)	24 (31%)	0	1 (1.3%)
Ectopia cordis	4 (3.2%)	1 (25%)	4 (1.2%)	1 (20%)	4 (100%)	3 (75%)	3 (75%)

*Numbers in parentheses represent the percentage of all families with the specific ultrasound presentation amongst all families with cardiovascular defects.
†Number of families for which ultrasound findings were confirmed by necropsy/histopathology of dead pups.
‡Numbers in parentheses represent the percentage of all abnormal fetuses with the specific ultrasound presentation amongst all fetuses with cardiovascular defects.
§Number of fetuses that were scanned on two or three different days.
¶Number of mutant fetuses that were also growth retarded, prenatal lethal, or exhibited bradycardia.
**Outflow velocity increase without outflow regurgitation.

fractional area change and shortening fraction. In many instances, heart failure was confirmed with the examination of dead pups, which typically showed congested heart, lung and liver (Table 1).

Outflow regurgitation is easily identified by color-flow Doppler analysis and is seen as an abnormal diastolic jet (orange flow, Fig. 1D) arising from the same vessel that has a systolic outflow (blue, Fig. 1C). Spectral Doppler analysis is then used to examine for an abnormal diastolic flow typical of semilunar valve regurgitation (Fig. 1E). Although outflow regurgitation was always associated with an increase in outflow velocity, 37 fetuses showed increased outflow velocity in the absence of outflow regurgitation, nine of which were also growth retarded and four died prenatally (Table 1).

Hypertrophy was detected using M-mode imaging and is defined as those fetuses with a wall thickness more than two standard deviations from the mean. Owing to difficulty in achieving the optimal imaging planes, M-mode data was obtained for less than 25% of the fetuses screened, and thus hypertrophy is underrepresented in the screen. Nevertheless, 23% of fetuses identified with heart defects exhibited hypertrophy (Table 1). This was observed in 77 fetuses from 44 families. The most infrequently observed defect was ectopia cordis, a condition where the heart develops outside the chest cavity. This is readily observed by 2D imaging, and was found in only 4 fetuses (Table 1).

Approximately 50% of the fetuses with outflow regurgitation and 25% of fetuses with other abnormal ultrasound presentations were ultrasound scanned two or three times on different days (Table 1). In almost all instances, the rescanning confirmed the original ultrasound presentations, sometimes even showing progression of the fetus into heart failure or death. Overall, excluding families exhibiting arrhythmias only, 61 (23%) families had serious cardiovascular defects. All affected fetuses died prenatally or at birth, except for some fetuses with isolated increased outflow velocity. By contrast, fetuses diagnosed with hypertrophy as the predominant defect all survived to term, but then expired at birth.

To obtain more specific diagnosis of the cardiovascular defects, whenever possible stillborn or dead pups were retrieved for necropsy and histological analysis (Table 1). Such

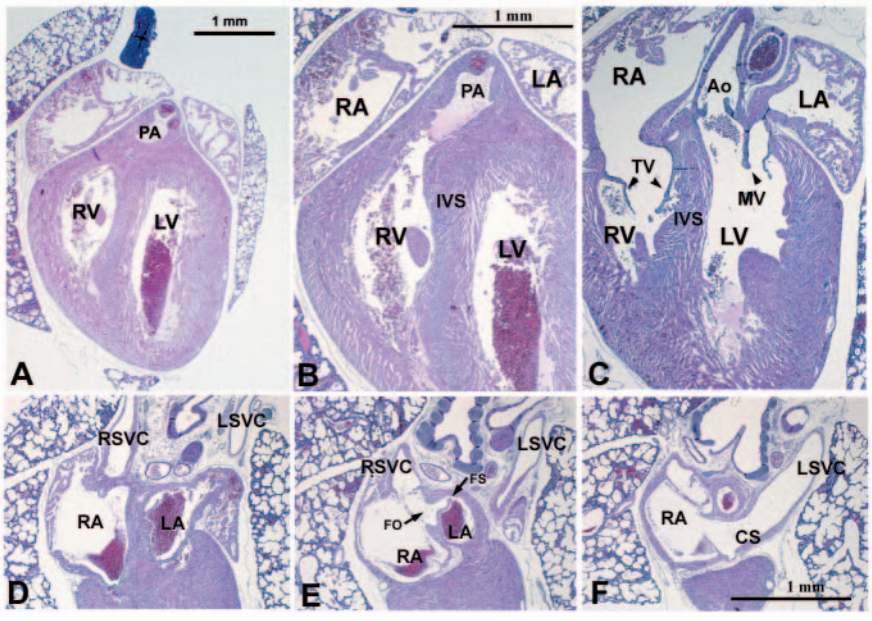

Fig. 2. Histological sections showing morphology of the normal neonatal mouse heart. (A) Low magnification view of the anterior portion of the heart, showing the normal configuration of the interventricular septum (IVS) and ventricular walls. Note the relative thickness of these components. (B,C) The right ventricular (RV) subpulmonary outflow tract (PA) is shown in B, whereas C illustrates the left ventricular (LV) outflow tract (Ao). Note the fibrous continuity of the mitroaortic valves. (D-F) Configuration of structures in the venous pole of the heart. The sequence of sections shows normal connection of the left superior vena cava (LSVC) to the right atrium (RA) via the coronary sinus (CS). Also shown are the right superior vena cava (RSVC) connection to the right atrium (RA; D,E) and the atrial septal complex. Same magnification used in panels B-F. MV, mitral valve; TV, tricuspid valve; FO, foramen ovale; FS, foramen secundum.

studies revealed a wide range of cardiovascular malformations, including persistent truncus arteriosus (PTA), transposition of the great arteries (TGA), double outlet right ventricle (DORV), Tetralogy of Fallot, pulmonary atresia, right-sided aortic arch, interrupted aortic arch (IAA), ventricular (VSD) and atrial (ASD) septal defects, common atrioventricular canal (AVC), pulmonary atresia, aortic stenosis, coronary artery defects, hypertrophy and hypoplastic left ventricle. Some of the mutant families exhibited cardiovascular defects in conjunction with craniofacial or skeletal anomalies, or limb defects. Below we present, by way of example, the detailed analyses of 5 families. To assist in the histological examination of the hearts from the mutant animals, we show in Fig. 2, histological sections of hearts from normal newborn mice.

Mutation causing persistent truncus arteriosus and craniofacial defects

Outflow regurgitation was associated with outflow alignment and/or septation defects in a number of ENU families. In family 26, the original ultrasound scan had indicated one fetus in a litter of six with outflow regurgitation. At birth, six pups were delivered, with one born dead. The dead pup exhibited craniofacial dysmorphism that included a pug nose, dome-shaped head, low-set ears, and short neck and limbs (Fig. 3A). Necropsy revealed that the fetus had PTA (Fig. 3D, compare with 3C) and also hypoplastic thymus. Histological analysis revealed a single great artery that gave rise to the coronary arteries, aorta and pulmonary arteries, with a short main pulmonary artery segment (‘type 1 1/2’ persistent truncus arteriosus). This heart also had an AVC with a primum ASD, VSD and atrioventricular valve abnormalities (Fig. 3G,H). The skeletal preparation showed micrognathia due to reduction in the premaxilla, maxilla, mandible and nasal bones. By contrast, the frontal bone was enlarged, accounting for the dome-shaped appearance of the head (Fig. 3E, compare with control in 3F).

To examine heritability and facilitate mapping of the mutation using polymorphic DNA markers, the G2 carrier female was intercrossed with C3H mice to generate C3H/C57BL6 hybrid offspring. Such studies showed the PTA phenotype was inherited in a recessive manner, being fully penetrant in presumptive homozygous offspring. Genome scan analysis using polymorphic microsatellite DNA markers mapped the mutation to mouse chromosome 2. This was carried out using the method of Neuhaus and Beier (Neuhaus and Beier, 1998) for recombinant haplotype interval analysis (Table 2; see Materials and methods). Using additional chromosome 2 markers, the map position was further narrowed to a 5 Mb interval between markers D2mit395 and D2mit398 (Table 3).

Transposition of the great arteries and heart situs anomalies

Family 182 exhibited outflow regurgitation, and was shown to have TGA, thymus hypoplasia and other heart situs anomalies (Fig. 4). Typically, affected fetuses show two parallel outflows positioned in an anterior/posterior arrangement, with the pulmonary trunk behind the aorta (Fig. 4C). Histological analysis showed the aorta connected to the RV, whereas the pulmonary outflow emerged from the LV (Fig. 4E-G). An AVC defect provided direct continuity between the atrial and ventricular chambers (Fig. 4H). An unusual coronary anomaly associated with the left coronary artery sinus ballooned into the ventricular septum (Fig. 4F,N). The right and left superior vena cava inserted symmetrically into the roof of the right and left atria, indicating right atrial isomerism (Fig. 4I; compare with Fig. 2D-F). Some fetuses had a ‘corrected’ TGA, associated with an inversion of the ventricles. Thus the aorta, positioned anterior to the pulmonary outflow, is connected to the morphological RV positioned on the left, whereas the pulmonary outflow connects to the morphological LV positioned on the right (Fig. 4K-N). In addition, a number of fetuses with TGA exhibited a right-sided aortic arch, and some also had ectopic pigmentation in the heart and chest cavity (Fig. 4J). Genome scanning of this family mapped the mutation causing TGA to distal mouse chromosome 4 (Table 2), and further refinement with additional markers narrowed the position to a 5.7 Mb interval between D4mit312 and D4mit189.

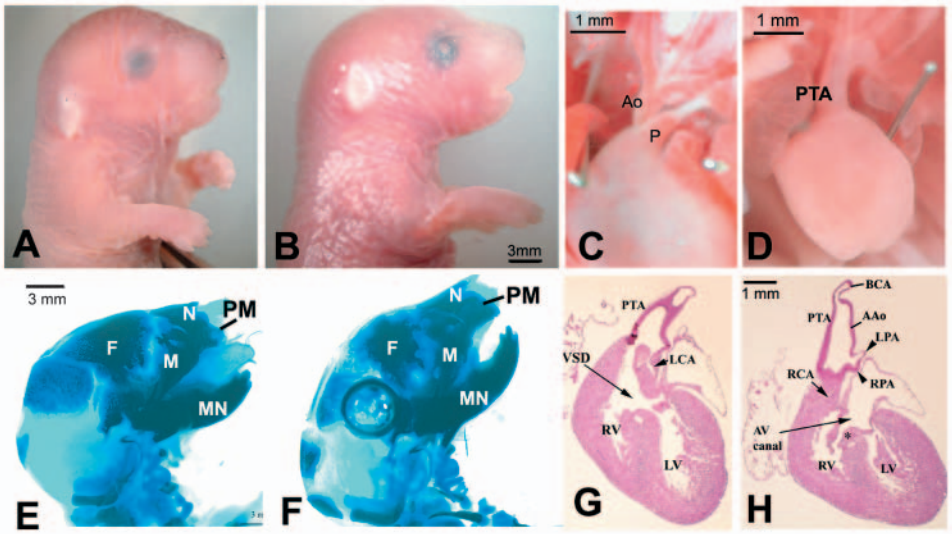

Fig. 3. Family 26 with persistent truncus arteriosus and craniofacial anomalies. (A) A pup that died at birth had a short snout, low set ears, rounded head, and short neck. (B) A normal neonatal C57BL6/J pup. Alcian blue staining (E,F) showed the abnormal pup (E) had a shortened premaxilla (PM), maxilla (M) and nasal bone (N), while its frontal bone (F) was expanded. The shape of the mandible (MN) was also altered. The heart exhibited persistent truncus arteriosus (PTA in D), when compared with normal septated outflows (C), consisting of an aortic (Ao) and pulmonary (P) trunk. Histological sections of the abnormal heart (G,H) revealed a single outflow positioned over the RV and VSD. This vessel gave rise to the ascending aorta (AAo) with its brachiocephalic artery (BCA), the right and left pulmonary arteries (RPA, LPA), and the coronary arteries (LCA, RCA). A VSD with inlet extension can be seen in (H). Asterisk in H denotes abnormal AV valve. Panels A and B, E and F, and G and H are shown at the same magnification.

Table 2. Mapping ENU-induced mutations using recombinant haplotype analysis

Chromosome interval*	Recombinant haplotypes† Family 26 (11)	Family 53 (9)	Family 166 (11)	Family 182 (8)
1-P	5	6	7	6
1-M	5	9	7	8
1-D	7	7	6	7
2-P	1‡	7	5	4
2-M	0	6	5	4
2-D	4	5	5	6
3-P	7	4	4	6
3-D	7	7	3	7
4-P	10	7	0	1
4-D	8	8	4	0
5	7	1	5	3
6-P	8	7	6	5
6-D	9	7	5	5
7	7	8	2	4
8	10	6	7	6
9	4	8	8	5
10	9	8	5	5
11	7	7	7	5
12	7	7	7	2
13	6	6	7	4
14	6	6	3	4
15	9	4	11	5
16	6	3	3	3
17	5	6	5	3
18	8	5	5	6
19	6	6	9	5
X-P	4	2	4	4
X-D	4	3	5	2

C57BL6/C3H offspring carrying the C57BL6-derived ENU-induced mutation were intercrossed and the resulting mutant offspring were genome scanned using 48 B6/C3H polymorphic DNA markers spanning the proximal and distal ends of each chromosome.

*For the six larger chromosomes, one or two internal markers were added, providing two or three chromosomal intervals for mapping. P, proximal; M, middle; D, distal.

†Recombinant haplotypes refer to number of C57BL6/C3H mutant offspring that show heterozygosity or homozygosity for C3H microsatellite markers on the respective chromosomes. Numbers in parentheses are the total number of mutant animals included in the initial genome scan.

‡Numbers in red indicate nonrecombinant haplotype intervals where mutation is likely situated.

Sema3C mutation causing persistent truncus arteriosus and aortic arch anomalies

Family 53 exhibited outflow regurgitation and was identified with PTA (Fig. 5). Typically, affected fetuses showed an undivided arterial outflow, together with an interrupted aortic arch (IAA) (Fig. 5A,C-E) or other arch anomalies, such as duplicated left carotid arteries (Fig. 5B). In some animals, the heart defects were accompanied by ectopic pigmentation in the heart, lung and other tissues in the chest cavity (Fig. 5L-N), while the skin showed hypopigmentation (Fig. 5F-K). The underlying ENU-induced mutation was mapped to the proximal region of chromosome 5 (Table 2), and further narrowed to a 13 Mb interval between markers D5mit193 and D5mit387 (Table 3). This interval contains a cluster of four semaphorin genes – *Sema3A*, *3C*, *3D* and *3E*. Of particular significance is the fact that *Sema3C* knockout mice have been described with a phenotype similar to that seen in this family, i.e. PTA with an interrupted aortic arch (Feiner et al., 2001). DNA sequencing confirmed a point mutation consisting of a T to C substitution that converted a leucine to proline (L605P) in the highly conserved immunoglobulin domain of Sema3C (Fig. 6). This single base change eliminated a *Pst*I restriction site, while adding an *Aci*I site, making it possible to use restriction digestions for rapid genotyping (Fig. 6).

Phenotype-genotype analyses surprisingly showed that some heterozygous $Sema3C^{L605P}$ mutants also have outflow anomalies. Thus, in a litter of 11 pups, three fetuses with PTA were homozygous for the *Sema3C* mutation, whereas one heterozygous animal had DORV (Fig. 6; also data not shown). Further analysis of an additional nine heterozygous $Sema3C^{L605P}$ fetuses or newborn pups showed that four were normal, two exhibited dysmorphic valves, two had DORV, and one had PTA/IAA. By contrast, analysis of 18 homozygous $Sema3C^{L605P}$ fetuses showed 13 with PTA/IAA and five with DORV. Given that heterozygous *Sema3C* knockout mice exhibit no phenotype, our findings would suggest that the $Sema3C^{L605P}$allele might exert dominant-negative effects. Interestingly, we found two homozygous $Sema3C^{L605P}$ mice that were adult viable, with one dying at 6 weeks of age with DORV. Such rare homozygous 'escapers' is perhaps not unexpected, as some *Sema3C* null mutants also survive to adulthood (Feiner et al., 2001).

Table 3. ENU-induced mouse mutations causing congenital heart defects

Family ID*	Phenotypes	Chromosome†	Map interval‡	DNA interval (*n*)§	Mutation recovered
53	PTA/IAA	5	D5mit193-D5mit387	13 Mb (9)	$Sema3C^{L605P}$
26	PTA Craniofacial	2	D2mit395-D2mit398	5 Mb (44)	Pending
182	TGA Situs defects	4	D4mit312-D4mit189	5.7 Mb (13)	Pending
166	VSD Syndactyly	4	D4mit196-D4mit288	17 Mb (32)	Pending
193	Conotruncal Coronary defect Craniofacial	10	NA	NA	$Gja1^{W45X}$

*Mutant mouse family identification.
†Mouse chromosome to which mutation was mapped.
‡Microsatellite DNA markers spanning the interval containing the mutation.
§*n*, total number of mutant animals used in mapping analyses.
NA, not analysed.

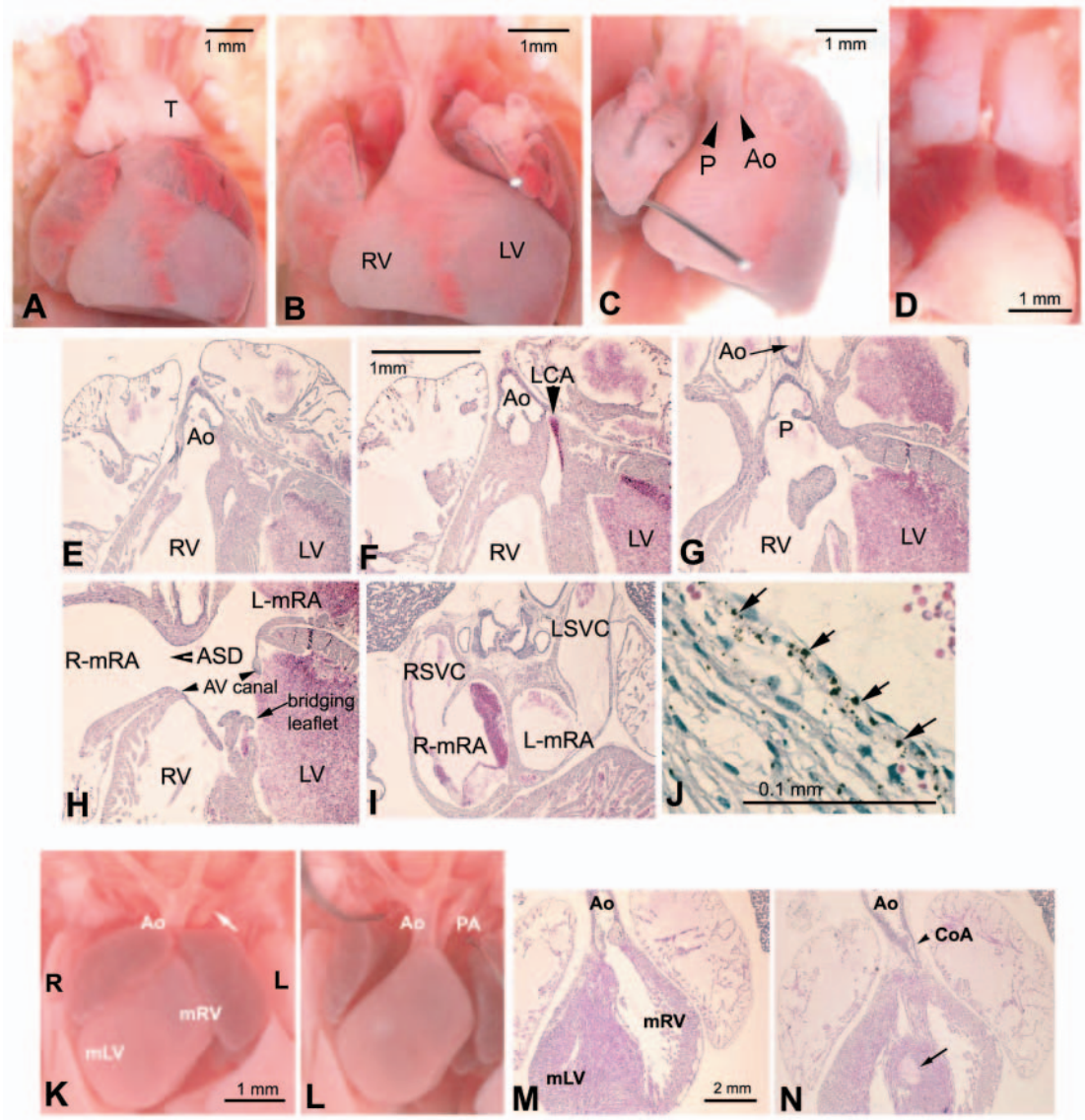

Fig. 4. Transposition of the great arteries and heart laterality defects in family 182. (A-D). A pup that died at birth showed thymic (T) hypoplasia (A) and an enlarged heart (A,B) with two thin outflows vessels positioned anterior-posterior (see arrowheads in C). For comparison, the chest cavity of a normal newborn mouse is shown in D. (E-J) Histological sections presented anterior to posterior (E-G) showed the aorta (Ao) positioned anteriorly (E), giving rise to the coronary arteries (F) and connecting to the RV (E). Lumen of the left coronary artery was enlarged (LCA). Panel G shows the pulmonary outflow (P) positioned posteriorly and a VSD. (H,I) Also observed is a primum ASD, single AV valve, canal type VSD (see canal in H), and bridging leaflet (arrow in H). Right atrial isomerism is indicated as the left-sided atrium (L-mRA) receives the left superior vena cava (LSVC) directly, while the right-sided atrium (R-mRA) receives the right superior vena cava (RSVC) in the normal fashion (I). (J) Ectopic pigment granules in the interventricular septum (arrows). (K-N) A fetal heart exhibited inverted ventricles together with right atrial isomerism. Apex of the heart is abnormally pointed to the right of the chest cavity (K,L). Arrow in K denotes the ductus arteriosus. The aortic (Ao) and pulmonary (PA) outflows are positioned anterior-posterior (L), with the anteriorly positioned aorta connected to the morphological right ventricle (mRV in M). A large coronary artery (CoA) drains into a sinusoidal fistula in the septum (see arrow in N). mLV, morphological left ventricle.

Connexin43 mutation causing conotruncal malformation and coronary anomalies

Family 193 showed outflow regurgitation together with an abnormal spectral Doppler signal that suggested hypertensive pulmonary outflow. Necropsy of dead pups revealed an unusual conotruncal malformation consisting of bulges or pouches at the base of the heart (Fig. 7A). In addition, defects involving the coronary arteries were evident. Most striking were coronary aneurysms found in the walls and at the base of the pulmonary and aortic outflows (Fig. 7B,C). In addition, typically a large peritruncal coronary vein was seen at the base of the outflows (Fig. 7B,C). Histological analysis showed that the conotruncal malformation consisted of sinusoidal trabeculations (Fig. 7E-G). In these regions and also in the RV chamber, there was marked thinning of the compact layer. Large subepicardial coronary vessels were observed, which were particularly abundant in the

peritruncal region of the heart (Fig. 7D-G). Some of these gave rise to large sinuses. In some instances, the coronary artery was observed to insert below the level of the valves (Fig. 7I). In addition, the semilunar valves were thickened (Fig. 7K), and a VSD can be seen (Fig. 7J). Among this constellation of phenotypes, the conotruncal malformation stands out as being reminiscent of the connexin43 knockout mouse (Reaume et al., 1995). Indeed, sequencing analysis confirmed a mutation in connexin43, a G to A substitution that generated a premature stop codon at amino acid position 45 (Fig. 7L; Table 3). The 44-amino acid polypeptide generated by this mutant *Gja1*^{W45X} allele is expected to terminate after the first transmembrane domain of connexin43, and thus would be incapable of forming a gap junction channel. It is interesting to note that the phenotype in the *Gja1*^{W45X} mutant is much more severe than that of the connexin43 knockout mouse. Although the mutation in this family was never formally mapped by genome scanning, the phenotype has been shown to segregate exclusively with the *Gja1*^{W45X} mutation. Thus in the fifth generation of breeding, we have found the same cardiovascular/pouch phenotype in 18 homozygote *Gja1*^{W45X} mutant animals.

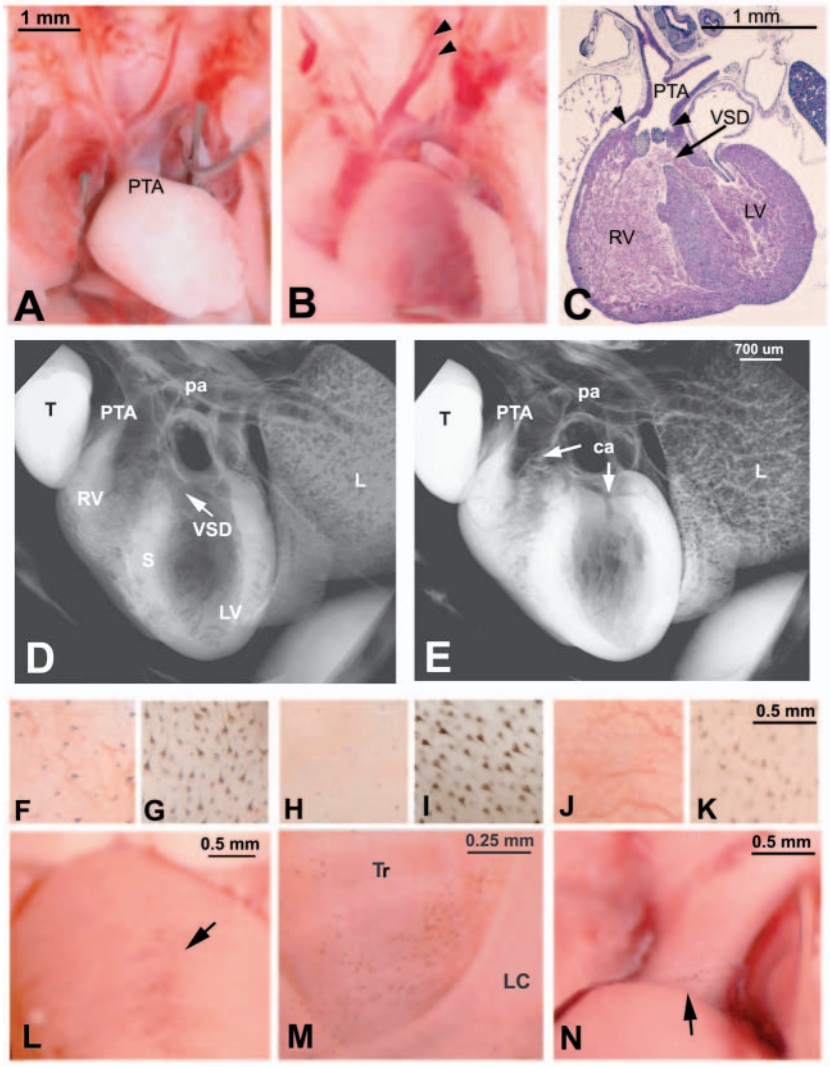

Fig. 5. Family 53 with outflow and aortic arch anomalies. (A-E). Persistent truncus arteriosus and DORV. Neonatal pups showed PTA together with IAA (A) or DORV with a duplicated left carotid artery (double arrowheads in B). Histology (C) and 3D reconstruction using episcopic fluorescence image capture (D,E) of a heart similar to that in shown in A revealed a single outflow tract that gave rise to the aorta and the pulmonary arteries (pa) and coronary arteries (ca) (arrowheads in C; white arrows in E). A VSD connects the RV and LV. L, lung; T, thymus. (F-K). Abnormal pigmentation. A homozygous *Sema3C*^{L605P} pup exhibited skin hypopigmentation (F,H,K), when compared with an age matched control pup (G,I,K). Shown is skin from head (F,G), trunk (H,I) and rump (J,K). Ectopic pigmentation is seen in the chest cavity (L-N), including the heart (arrow, L), lung (not shown), trachea (Tr, M) and great vessels (arrow in N). LC, left carotid artery.

Heart and forelimb defects

In family 166, heart defects were observed in conjunction with forelimb defects, phenotypes that are reminiscent of Holt-Oram syndrome. Ultrasound phenotyping had indicated regurgitant flow and hypertrophy, heart failure and growth retardation. The affected pups died at birth and typically had forelimbs that were abnormally flexed towards the chest (Fig. 8A,B) and with clubbed paws. Usually the front paws had only three digits (Fig. 8B), or three digits with the third digit showing bifurcation (Fig. 8C,D). Necropsy revealed congested atria, large peritruncal coronary veins at the base of the outflows, and indications of hypertrophy (Fig. 8F,G). Histological analysis confirmed biventricular hypertrophy (Fig. 8H,J,L; compare with control in Fig. 2A), small muscular VSDs (Fig. 8J-P), variable coronary (Fig. 8E,G,H; compare with Fig. 2A,B) and myocardial anomalies (Fig. 8E,I,K,M; compare with Fig. 2B,C). Given the presence of a patent foramen ovale in newborn pups, it was difficult to assess for the presence of ASDs. Interestingly, some heterozygous mutants also exhibited similar heart defects to those seen in homozygous mutants, but no obvious forelimb anomalies (Fig. 8E,H,I). Analysis by genome scanning mapped the ENU-induced mutation in this family to mouse chromosome 4 (Table 2), and with additional markers, this has been localized to a 17 Mb interval between markers D4mit196 and D4mit288 (Table 3).

Discussion

We showed that non-invasive ultrasound imaging is highly effective in phenotyping mouse fetuses for congenital cardiovascular anomalies. This method is high throughput, and allows the assessment of both cardiovascular structure and function. The defects found included most of the major congenital heart anomalies seen clinically. Using a genome-wide scan with microsatellite DNA markers, we mapped the mutations in five families, and identified the mutant genes in two of these families as *Sema3C*^{L605P} and *Gja1*^{W45X}.

In family 26, PTA was observed in conjunction with thymus hypoplasia, micrognathia and other craniofacial defects –

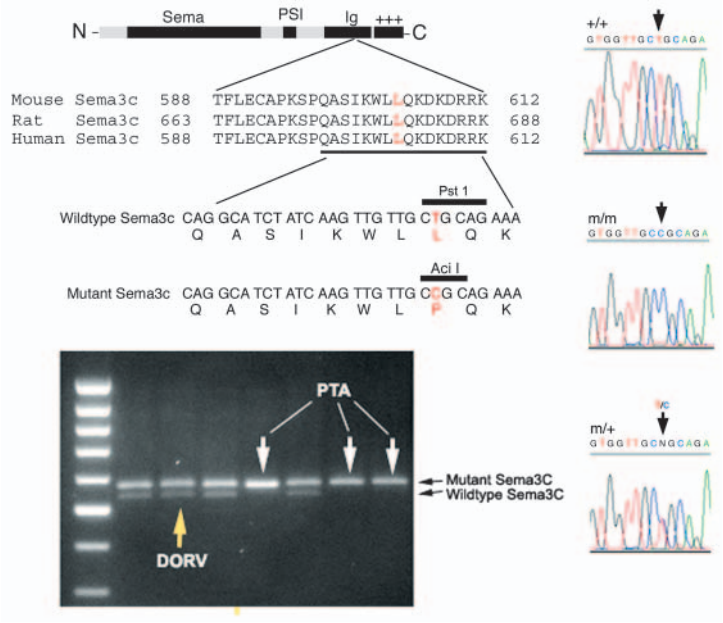

Fig. 6. Mutation in a highly conserved *Sema3C* immunoglobulin domain. Family 53 pups with PTA are homozygous for a T to C substitution (m/m sequencing trace files, right) in the highly conserved immunoglobulin (Ig) domain of *Sema3C*, which caused a leucine to proline substitution, and also resulted in the loss of a *Pst*I restriction site and the gain of an *Aci*I site. PCR amplification using primers spanning the $Sema3C^{L605P}$ mutation, followed by *Pst*I digestion was used to genotype a litter of fetuses obtained from intercrossing two heterozygous $Sema3C^{L605P}$ mutants (see bottom gel). Three homozygous $Sema3C^{L605P}$ mutants showed PTA, whereas one heterozygous fetus had DORV.

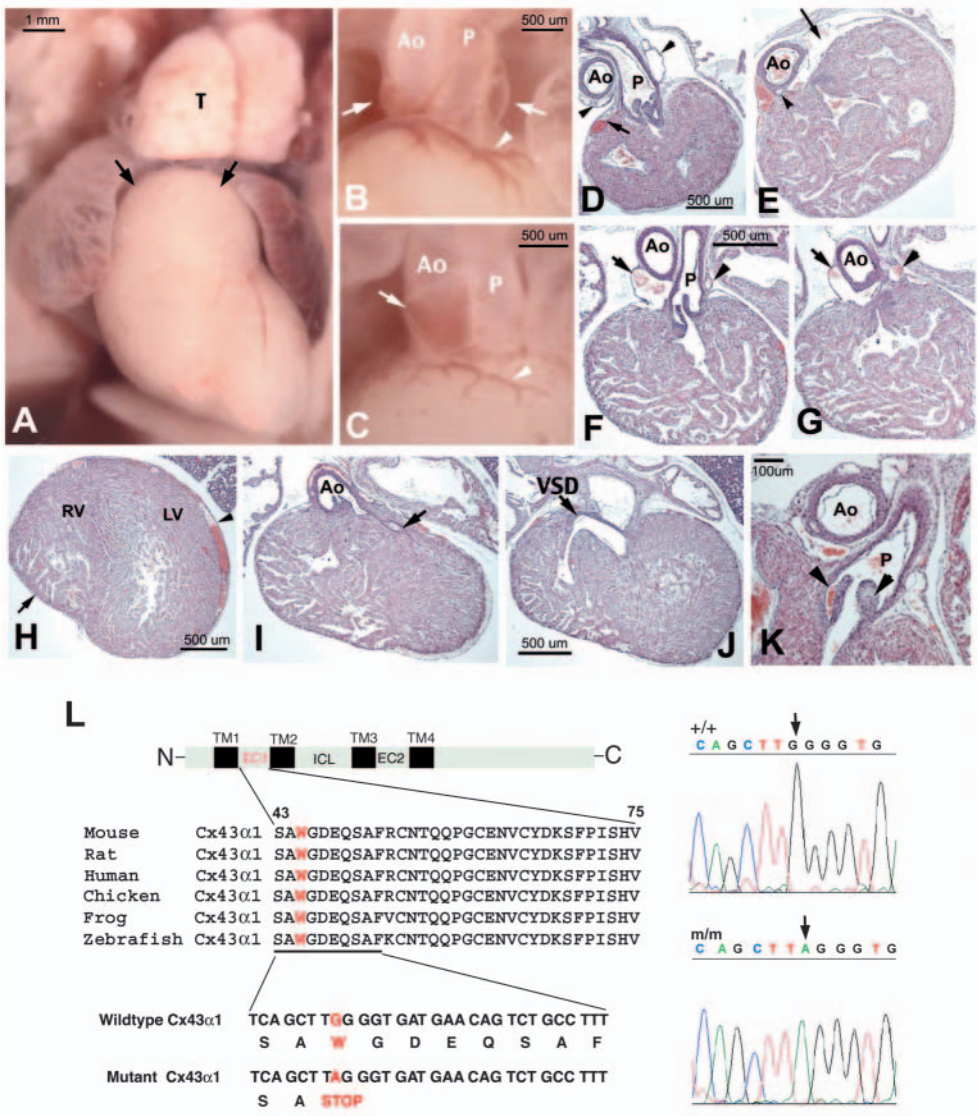

Fig. 7. Conotruncal heart defects and coronary anomalies elicited by a novel connexin43 mutation. (A-G) Conotrucal bulge (black arrows in A) and hypoplastic thymus (T) are evident in this homozygous $Cx43^{W45X}$ pup. At the base of the outflows is a prominent peritruncal coronary vessel (white arrowhead in panels B,C), and coronary aneurysms are seen in the wall of the aortic and pulmonary outflows (white arrows in panels B,C). These can be seen in histological sections (D-G). Also note sinusoidal trabeculae at the base of the outflow (E-G). Arrowhead in D and arrows in E-G denote coronary aneurysms, and arrow in D and arrowheads in E-G denote abnormal coronary plexuses. (H-K). Histology shows a large subepicardial coronary vessel (arrowhead in D) and an abnormally thinned compact layer (arrow in H). In one heart, a coronary artery inserts into the aorta below the level of the valves (I), and enlarges to form a sinus (arrow in panel I). Also observed are a VSD (J) and thickened valves (arrowheads, K). (L) Protein structure of connexin43 is shown on the left, indicating four transmemebrane (TM1, 2, 3 and 4) domains, two extracellular loops (EC1 and 2) and an intracellular loop (ICL). The region spanning EC1 is highly conserved in vertebrates. Sequence trace files (right) revealed a G to A substitution that generated a STOP codon at amino acid 45, which normally encodes tryptophan (W).

phenotypes that are reminiscent of DiGeorge and velocardiofacial syndromes. Previous knockout mouse studies showed that *Tbx1* and *CRKL*, two genes situated in the syntenic region of chromosome 22, which is deleted in DiGeorge patients, have cardiovascular and craniofacial defects similar to those in DiGeorge patients (Lindsay et al., 2001; Jerome and Papaioannou, 2001; Merscher et al., 2001; Guris et al., 2001). In addition, antisense attenuation of *UFD1L*, another gene in this region, has been associated with outflow septation defects in chick embryos (Yamagishi et al., 2003). However, some DiGeorge patients have a 10p rather than 22q11 chromosomal deletion, suggesting there is at least one additional DiGeroge locus (Monaco et al., 1991; Schuffenhauer et al., 1998; Van Esch et al., 1999). Yet other DiGeorge patients show no detectable chromosome deletions (Lichtner et al., 2002). DNA sequencing analysis of many such patients showed most have no detectable mutation in the *Tbx1* coding sequence (Gong et al., 2001; Conti et al., 2003; Yagi et al., 2003). The mutation in family 26 is situated on mouse chromosome 2, in a 5-Mb region containing 124 known or predicted genes. Although mouse chromosome 2 contains regions of synteny with human 10p, this interval appears largely syntenic to human chromosome 15.

In family 166, VSDs were linked with forelimb anomalies that included oligodactyly and syndactyly, and possibly other radial ray defects (indicated by the abnormal flexure of the forearm). These phenotypes are reminiscent of those in Holt-Oram syndrome, which has been linked with *TBX5* mutations (Basson et al., 1997; Li et al., 1997b). We note that studies using a *Tbx5* knockout mouse model showed ASD and VSD, and subtle defects of the front paw and wrist in some of the heterozygous knockout animals (Bruneau et al., 2001). The mutation in family 166 was mapped to mouse chromosome 4, which does not contain *Tbx5* nor *Sall4*, the two genes linked with Holt-Oram or the closely related Okihiro syndromes, respectively (Basson et al., 1997; Li et al., 1997b; Kohlhase et al., 2002). Clinical studies have shown that 30-70% of patients with Holt-Oram syndrome have mutations in *Tbx5* (Cross et al., 2000; Mori and Bruneau, 2004), leaving open the possibility that the mutation in family 166 may have a relevance for Holt-Oram syndrome.

The mutation in family 182 exhibiting TGA was mapped to chromosome 4, which has a strong candidate gene, *Hspg2*, encoding the heparan sulfate proteoglycan perlecan. Previous studies showed perlecan knockout mouse surviving past E10.5-

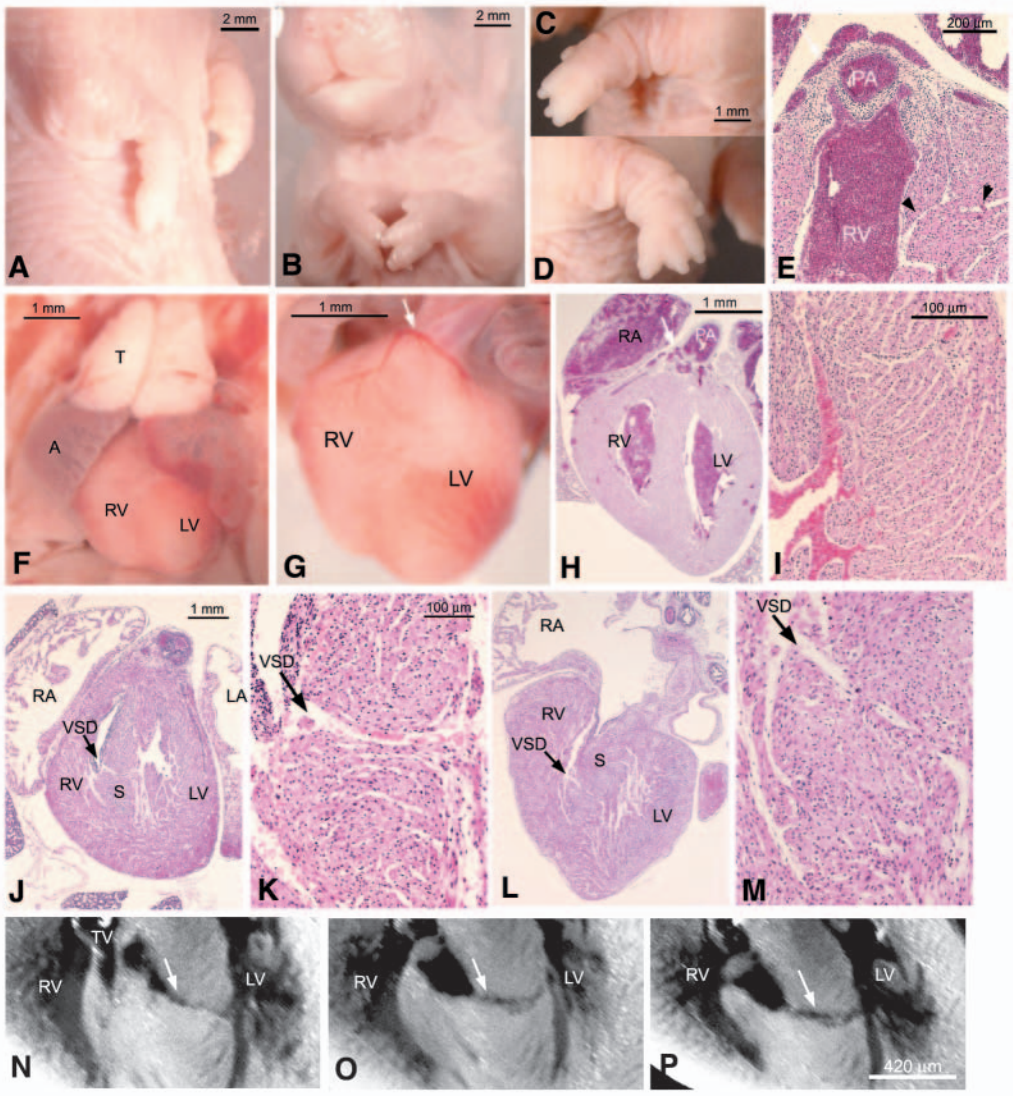

Fig. 8. Forelimb and heart defects in Family 166. (A-D) Forelimbs are abnormally flexed towards the chest, with clubbed front paws. Typically three digits are seen (B), but in some pups, there appears to be a fusion of the third and fourth digits (C,D). (F,G) Whole-mount view shows enlarged atria and an abnormal heart shape indicative of hypertrophy (F,G). An abnormal large peritruncal coronary vein is observed at the base of the outflows (white arrow, G). (E,H-M) Histology shows biventricular hypertrophy (H,J,L), and abnormal coronaries around the outflow vessels (E, white arrow in H). Also evident are muscular VSDs (see arrows in J-M), and disorganized myocardium (E,I,K,M), which frequently shows gaps between the myofiber bundles (see arrowhead in E). (N-P) The heart shown in (G) was processed for episcopic fluorescence image capture, and the image stacks obtained were re-sectioned at a different pitch to visualize the VSDs (see white arrows). Sections in E, H and I are from heterozygous, whereas the rest are from homozygous animals.

E11 can exhibit TGA (Costell et al., 1999; Hirasawa et al., 1999; Costell et al., 2002). However, fine mapping studies have narrowed the interval to a 5.7 Mb segment on chromosome 4 that does not include *Hspg2*. We note that unlike the perlecan knockout mouse, mutants in family 182 exhibit heart situs anomalies never seen in the perlecan knockout mouse (Costell et al., 2002). Besides *Hspg2*, there are only two other genes known to be associated with TGA, cryptic, a member of the EGF-CFC family of membrane receptors (Gaio et al., 1999), and activin receptor type IIB (Oh and Li, 1997). Neither of these genes are situated on chromosome 4, suggesting that the mutation in family 182 may correspond to a novel gene not previously known to be associated with TGA and the specification of laterality.

Semaphorin 3C mutation

The PTA and IAA defects in family 53 were shown to arise from a point mutation in *Sema3C*. The $Sema3C^{L605P}$ mutation causes a non-conservative amino acid substitution in the immunoglobulin domain, a protein region previously shown to be dispensable for biological activity (Koppel et al., 1997). Nevertheless, the high degree of sequence conservation in this protein domain would suggest an essential function. As semaphorins are known to function as dimers, perhaps this immunoglobulin domain may have a role in semaphorin dimerization (Koppel and Raper, 1998). Consistent with this possibility, previous studies showed that replacement of the immunoglobulin domain in Sema3A with the Fc domain of IgG allowed the retention of semaphorin activity (Eickholt et al., 1999). If indeed this mutation interferes with protein dimerization, homozygous mutant animals would expected to be functional nulls, which would explain why they have phenotypes similar to the Sema3C knockout animals. At the same time, it would predict that Sema3C activity may be reduced in heterozygote animals because of dominant interference with protein dimerization. The latter could account for the finding of cardiovascular defects in heterozygous $Sema3C^{L605P}$ mutants.

The semaphorin family of proteins, including Sema3C, provide guidance cues for axon pathfinding, and also has been suggested to play an important role in modulating neural crest cell migration (Kolodkin et al., 1993; Luo et al., 1993; Eickholt et al., 1999; Brown et al., 2001) (for a review, see Tamagnone and Comoglio, 2004). Sema3C is found along the migratory paths of cardiac neural crest cells, and cardiac neural crest cells express plexinA2, a co-receptor mediating semaphorin signaling (Brown et al., 2001). As deployment of neural crest cells to the heart plays an essential role in aortic arch remodeling and outflow tract septation (Hutson and Kirby, 2003), it is significant that cardiac neural crest abundance appears to be reduced in the *Sema3C* knockout mouse embryo (Brown et al., 2001). In conjunction with the cardiac phenotype, we also observed pigmentation defects in the $Sema3C^{L605P}$ mutant – ectopic pigmentation in the chest cavity in conjunction with skin hypopigmentation. As *Sema3C* transcripts are expressed in the ectoderm (Chilton and Guthrie, 2003), this suggests a previously unknown role for *Sema3C* in targeting and/or maintaining crest-derived melanocyte precursors in the skin.

ENU-induced connexin43 mutation

Another ENU-induced mutation identified is the connexin43 allele $Cx43^{W45X}$. This mutation generated a premature stop codon at amino acid 45, resulting in a hypothetical 44-amino acid polypeptide that spans the first transmembrane domain, ending shortly after the first extracellular loop. This N-terminal truncated connexin43 polypeptide cannot form a gap junction channel, which probably requires all four transmembrane domains, as well as the two extracellular loops that mediate docking of the gap junction hemichannels (Foote et al., 1998). Although this mutation might be predicted to be a functional null, the cardiovascular phenotype is more severe than that of the connexin43 knockout mouse. Thus the coronary aneurysms, VSD and semilunar valve abnormalities have never been seen in the connexin43 knockout mouse. This difference is unlikely to be caused by strain background effects, as we have maintained the connexin43 knockout mouse line in a C57BL6/J background. These findings suggest that the N-terminal polypeptide encoded by $Cx43^{W45X}$ may exert dominant-negative effects, such as via heteromeric interactions with other connexin polypeptides. The N-terminal polypeptide also may interact with other membrane or cytoplasmic proteins, an intriguing possibility given the evidence for protein-protein interactions involving the C terminus of connexin43 and a variety of other proteins, such as ZO1, β-catenin, and others (Toyufuku et al., 1998; Ai et al., 2000; Giepmans et al., 2001a; Giepmans et al., 2001b). Our previous studies have indicated that the conotruncal heart defects in the connexin43 knockout mouse arises from perturbations in the migratory behavior of two extracardiac cell populations, the cardiac neural crest and proepicardially derived cells (Huang et al., 1998a; Huang et al., 1998b; Li et al., 2002). Using this new connexin43 mutant mouse model, we hope to further elucidate connexin43 structure-function relationships and the mechanism through which connexin43 regulates neural crest and proepicardial cell motility.

Dominant and recessive inheritance

Our mutagenesis screen was designed to recover recessive mutations, with the expectation that this would increase the sensitivity of the screen in uncovering mutations causing severe congenital heart defects. This expectation was in fact realized. However, mutations causing human congenital heart disease are largely autosomal dominant. This disparity could partly reflect the bias inherent in a recessive screen, or perhaps gene dosage regulation in mouse is different than in human. We note that mice with homozygous *Tbx1* deficiency have DiGeorge-like outflow anomalies, but no outflow anomalies were found in heterozygous mutants; these mice showed mostly mild defects involving derivatives of the fourth pharyngeal arch (Jerone and Papaioannou, 2001; Lindsay et al., 2001; Merscher et al., 2001). However, it is also probably the case that recessive mutations causing human congenital heart disease are difficult to recover, as the incidence of pairing required to generate homozygote offspring in a randomly breeding population is likely to be very low. In addition, as most ENU-induced mouse mutations causing serious heart defects caused prenatal or neonatal lethality, this might predict early miscarriages that would be missed in clinical studies of live births (given a term mouse fetus is developmentally equivalent to a 8-9 weeks gestation human embryo). Finally, we note that in fact heterozygous offspring in a number of our ENU families have cardiovascular defects. This was observed

for the heart defects in family 166, and the outflow septation and arch anomalies elicited by the *Sema3C*^{L605P} mutation in family 53. These observations suggest that ENU-induced mutations will be invaluable in providing novel insights into gene function, and in some cases, may provide mutant alleles that may more closely model the genetics of human congenital heart disease.

Future prospects for ENU mutagenesis

Our ongoing screen has recovered mutants with a variety of other cardiovascular phenotypes. These new mouse models undoubtedly will help to define developmental pathways that play an essential role in congenital heart disease. We anticipate recovering not only novel alleles of known genes, but also novel genes that play a role in a wide variety of congenital heart defects. In contrast to analysis in human pedigrees, mouse models provide the opportunity to examine phenotype-genotype correlations in well-defined genetic backgrounds. This may make it possible to test for multigenic contributions, as well as the role of gene-environment interactions in congenital heart disease. Such studies may provide some insights into the often-observed variable penetrance and genetic heterogeneity associated with human congenital heart disease.

We thank J. Raper, J. Epstein and W. Pavan for helpful discussions; C. Coleman for skeletal preparations; J. Cash, H. Di'Medici, J. Noor and H. Dudik for animal husbandry; and A. Phelps and I. Moralez for assistance in histology. This work was supported by grants to C.W.L. (ZO1-HL005701), K.S. (HL66611), A.W. (NIH-P01-HD39946, NIH-P01-HL52813 and AHA-GIA995099U), J.F.L. (NIH-T32-HL07710) and M.L.K. (HL36059, HL70140, HD39946).

References

Ai, Z., Fischer, A., Spray, D. C., Brown, A. M. and Fishman, G. I. (2000). Wnt-1 regulation of connexin43 in cardiac myocytes. *J. Clin. Invest.* **105**, 161-171.

Basson, C. T., Bachinsky, D. R., Lin, R. C., Levi, T., elkins, J. A., Soults, J., Grayzel, D., Kroumpouzou, E., Traill, T. A., Leblanc-Straceski, J. et al. (1997). Mutations in human Tbx5 cause limb and cardiac malformation in Holt-Oram syndrome. *Nat. Genet.* **15**, 30-35.

Brown, C. B., Feinter, L., Lu, M. M., Ma, X., Webber, A. L., Jia, L., Rapear, J. A. and Epstein, J. A. (2001). PlexinA2 and sempahorin signaling during cardiac neural crest developoment. *Development* **128**, 3071-3080.

Bruneau, B. G., Nemer, G., Schmitt, J. P., Charron, F., Robitaille, L., Caron, S., Conner, D. A., Gessler, M., Nemer, M., Seidman, C. E. et al. (2001). A murine model of Holt-Oram syndrome defines roles of the T-box transcription factor Tbx5 in cardiogenesis and disease. *Cell* **106**, 709-721.

Chilton, J. K. and Guthrie, S. (2003). Cranial expression of class 3 secreted semaphorins and their neuropilin receptors. *Dev. Dyn.* **228**, 726-733.

Conti, E., Grifone, N., Sarkozy, A., Tandoi, C., Marino, B., Digilio, M. C., Mingarelli, R., Pizzuti, A. and Dallapiccola, B. (2003). DiGeorge subtypes of nonsyndronmic conotruncal defects: evidence againt a major role of TBX1 gene. *Eur. J. Hum. Genetic* **11**, 349-351.

Costell, M., Gustafasson, E., Aszodi, A., Morgelin, M., Bloch, W., Hunziker, E., Addicks, K., Timpl, R. and Fassler, R. (1999). Perlecan maintains the integrity of cartilage and some basement membranes. *J. Cell Biol.* **147**, 1109-1122.

Costell, M., Carmona, R., Gustafsson, E., Gonzalez-Iriarte, M., Fassler, R. and Munoz-Chapuli, R. (2002). Hyperplastic conotruncal endocardial cushions and transposition of great arteries in perlecan-null mice. *Circ. Res.* **91**, 158-164.

Cross, S. J., Ching, Y. H., Li, Q. Y., Armstrong-Buisseret, L., Spranger, S., Lyonnet, S., Bonnet, D., Penttinen, M., Jonveaux, P., Leheup, B. et al. (2000). The mutation spectrum in Holt-Oram syndrome. *J. Med. Genet.* **37**, 785-787.

Eickholt, B. J., Mackenzie, S. L., Graham, A., Walsh, F. S. and Doherty, P. (1999). Evidence for collapsing-1 function in the control of neural crest migration in both trunk and hindbrain regions. *Development* **162**, 2181-2189.

Favor, J. (1986). The frequency of dominant cataract and recessive specific-locus mutations in mice derived from 80 or 160 mg ethylnitrosourea per kg body weight treated spermtaogonia. *Mutat. Res.* **162**, 69-80.

Feiner, L., Webber, A. L., Brown, C. B., Lu, M. M., Feinstein, P., Mombaerts, P., Epstein, J. A. and Raper, J. A. (2001). Targeted disruption of semaphoring 3C leads to persistent truncus arteriosus and aortic arch interruption. *Development* **128**, 3061-3070.

Foote, C. I., Zhou, L., Zhu, X. and Nicholson, B. J. (1998). The pattern of disulfide linkages in the extracellular loop regions of connexin32 suggests a model for the docking interace of gap junctions. *J. Cell Biol.* **140**, 1187-1197.

Gaio, U., Schweickert, A., Fischer, A., Garratt, A. N., Muller, T., Ozcelik, C., Lankes, W., Strehle, M., Britsch, S., Blum, M. et al. (1999). A role of the cryptic gene in the correct establishment of the left-right axis. *Curr. Biol.* **9**, 1339-1342.

Garg, V., Kathiriya, I. S., Barnes, R., Schluterman, M. K., King, I. N., Butler, C. A., Rothrock, C. R., Eapen, R. S., Hirayama-Yamada, K., Joo, K. et al. (2003). GATA4 mutations cause human congenital heart defects and reveal an interaction with Tbx5. *Nature* **424**, 443-447.

Gebbia, M., Ferrero, G. B., Pilia, G., Bassi, M. T., Aylsworth, A., Penman-Splitt, M., Bird, L. M., Bamforth, J. S., Burn, J., Schlessinger, D. et al. (1997). X-linked situs abnormalties result from mutations in ZIC3. *Nat. Genet.* **17**, 305-308.

Giepmans, B. N., Hengeveld, T., Postma, F. R. and Moolenaar, W. H. (2001a). Interaction of c-Src with gap junction protein connexin-43. Role in the regulation of cell-cell communication. *J. Biol. Chem.* **276**, 8544-8549.

Giepmans, B. N., Verlaan, I., Hengeveld, T., Janssen, H., Calafat, J., Falk, M. M. and Moolenaar, W. H. (2001b). Gap junction protein connexin-43 interacts directly with microtubules. *Curr. Biol.* **11**, 1364-1368.

Gong, W., Gottlieb, S., Colins, J., Blescia, A., Dietz, H., Goldmuntz, E., McDonald-McGinn, D. M., Zackai, E. H., Emmanuel, B. S., Driscoll, D. A. et al. (2001). Mutation analysis of TBX1 in nondeleted patients with features of DGS/VCFS or isolated cardiovascular defects. *J. Med. Genet.* **38**, E45.

Gui, Y.-H., Linask, K., Khowsathit, P. and Huhta, J. (1996). Doppler echocardiography of normal and abnormal embryonic mouse heart. *Ped. Res.* **40**, 633-642.

Guris, D. L., Fantes, J., Tara, D., Druker, B. J. and Imamoto, A. (2001). Mice lacking the homologue of the human 22q11.2 gene CRKL phenocopy neurocristopathies of DiGeorge syndrome. *Nat. Genet.* **27**, 293-298.

Hirawsawa, E. A., Watanabe, H., Takami, H., Hassell, J. R. and Yamada, Y. (1999). Perlecan is essential for cartilage and cephalic development. *Nature* **23**, 354-358.

Hoffman, J. I. E. (1995). Incidence of congenital heart disease. II. Prenatal incidence. *Pediatr. Cardiol.* **16**, 155-165.

Hoffman, J. I. E. and Kaplan, S. (2002). The incidence of congenital heart disease. *Pediatr. Cardiol.* **39**, 1890-1900.

Huang, G. Y., Cooper, E. S., Waldo, K., Kirby, M. L., Gilula, N. B. and Lo, C. W. (1998a). Gap junction mediated cell-cell communication modulates mouse neural crest migration. *J. Cell Biol.* **143**, 1725-1734.

Huang, G., Wessels, A., Smith, B., Linask, K., Ewart, J. and Lo, C. (1998b). Alteration in connexin 43 gap junction gene dosage impairs conotruncal heart development. *Dev. Biol.* **198**, 32-44.

Hutson, M. R. and Kirby, M. L. (2003). Neural crest and cardiovascular development: a 20 year perspective. *Birth Defects Res. Part C. Embryo Today* **69**, 2-13.

Jerome, L. and Papaioannou, V. (2001). DiGeorge syndrome phenotype in mice mutant for the T-box gene, Tbx1. *Nat. Genet.* **27**, 286-240.

Jira, P. E., Waterham, H. R., Wanders, R. J. A., Smeitink, J. A. M., Sengers, R. C. A. and Wevers, R. A. (2003). Smith-Lemli-Opitz syndrome and the DHCR7 gene. *Ann. Human Genet.* **67**, 269-280.

Kohlhase, J., Heinrich, M., Schubert, L., Liebers, M., Kispert, A., Laccone, F., Turnpenny, P., Winter, R. M. and Reardon, W. (2002). Okihiro syndrome is caused by SALL4 mutations. *Hum. Mol. Genet.* **23**, 2979-2987.

Kolodkin, A. L., Matthes, D. I. and Goodman, C. S. (1993). The semaphoring genes encode a family of transmembrane and secreted growth cone guidance molecules. *Cell* **75**, 1389-1399.

Koppel, A. M. and Raper, J. A. (1998). Collapsin-1 covalently dimerizes,

and dimerization is necessary for collapsing activity. *J. Biol. Chem.* **273**, 15708-15713.

Koppel, A. M., Feiner, L., Kobayashi, H. and Raper, J. A. (1997). A 70 amino acid region within the semaphorin domain activates specific cellular response of semaphoring family members. *Neuron* **19**, 531-537.

Leatherbury, L., Yu, Q. and Lo, C. W. (2003). Noninvasive phenotypic analysis of cardiovascular structure and function in fetal mice using ultrasound. *Birth Defects Res. Part C Embryo Today* **69**, 83-91.

Li, L., Krantz, I. D., Deng, Y., Genin, A., Banata, A. B., Collins, C. C., Qi, M., Trask, B. J., Kuo, W. L., Cochran, J. et al. (1997a). Alagille syndrome is caused by mutations in human Jagged1, which encodes a ligand for Notch1. *Nat. Genet*. **16**, 243-251.

Li, Q. Y., Newbury-Ecob, R. A., Terrett, J. A., Wilson, D. I., Curtis, A. R., Yi, C. H., Gebuhr, T., Bullen, P. J., Robson, S. C., Strachan, T. et al. (1997b). Holt-Oram syndrome is caused by mutations in Tbx5, a member of the Brachyury (T) gene family. *Nat. Genet.* **15**, 21-29.

Li, W. E. I., Waldo, K., Linask, K. L., Chen, T., Wessels, A., Parmacek, M. S., Kirby, M. L. and Lo, C. W. (2002). An essential role for connexin43 gap junctions in mouse coronary artery development. *Development* **129**, 2031-2042.

Lichtner, P., Attie-Bitach, T., Schuffenhauer, S., Henwood, J., Bouvagnet, P., Scambler, P. J., Meitinger, T. and Vekemans, M. (2002). Expression and mutation analysis of BRUNOL3, a candidate gene for heart and thymus developmental defects associated with partial monosomy 10P. *J. Mol. Med.* **81**, 431-442.

Lindsay, E. A., Vitelli, F., Su, H., Morishima, M., Huynh, T., Pramparao, T., Jurecic, V., Ogunrinu, G., Sutherland, H. F., Scambler, P. J. et al. (2001). Tbx1 haploinsufficiency in the DiGeorge syndrome region causes aortic arch defects in mice. *Nature* **410**, 97-101.

Luo, Y., Raible, D. and Raper, J. A. (1993). Collapsin: a protein in brain that induces the collapse and paralysis of neuronal growth cones. *Cell* **75**, 217-227.

Maki, J. M., Rasanen, J., Tikkanen, H., Sormunen, R., Makikallio, K. I., Kivirikko, K. I. and Soininen, R. (2002). Inactivation of the lysyl oxidase gene Lox leads to aortic aneurysms, cardiovascular dysfunction, and perinatal death in mice. *Circulation* **106**, 2503-2509.

Merscher, S., Funke, B., Epstein, J., Heyer, J., Puech, A., Lu, M., Xavier, R., Demay, M., Russell, R., Factor, S. et al. (2001). *Tbx1* is responsible for cardiovascular defects in velo-cardio-facial/DiGeorge syndrome. *Cell* **104**, 619-629.

Monaco, G., Pignata, C., Rossi, E., Mascarello, O., Cocozza, S. and Ciccimarra, F. (1991). DiGeorge anomaly associated with 10p deletion. *Am. J. Med. Genet.* **39**, 215-216.

Mori, A. D. and Bruneau, B. G. (2004). Tbx5 mutations and congenital heart disease: Holt-Oram syndrome revealed. *Curr. Opin. Cardiol.* **19**, 211-215.

Neuhaus, I. and Beier, D. (1998). Efficient localization of mutations by interval haplotype analysis. *Mamm. Genome* **9**, 150-154.

Oda, T., Elkahloun, A. G., Pike, B. L., Okajima, K., Krantz, I. D., Genin, A., Piccoli, D. A., Meltzer, P. S., Spinner, N. B., Collins, F. S. et al. (1997). Mutations in the human Jagged 1 gene are responsible for Alagille syndrome. *Nat. Genet.* **16**, 235-242.

Oh, S. P. and Li, E. (1997). The signaling pathway mediated by the type IIB activin receptor contorlws axial patterning and lateral asymmetry in the mouse. *Genes Dev.* **11**, 1812-1826.

Pickard, G., Sollars, P., Rinchik, E., Nolan, P. and Bucan, M. (1995). Mutagenesis and behaviorial screening for altered circadian activity identifies the mouse mutant, Wheels. *Brain Res.* **705**, 255-266.

Reaume, A. G., de Sousa, P. A., Kulkarni, S., Langille, B. L., Zhu, D., Davies, T. C., Juneja, S. C., Kidder, G. M. and Rossant, J. (1995). Cardiac malformation in neonatal mice lacking connexin43. *Science* **267**, 1831-1834.

Rosenthal, G. (1998). Prevalence of congenital heart disease. In *The Science and Practice of Pediatric Cardiology*, 2nd Edition, pp. 1083-1105. Baltimore, MD: Lippincott Williams & Wilkins.

Satoda, M., Zhao, F., Diaz, G. A., Burn, J., Goodship, J., Davidson, H. R., Pierpont, M. E. M. and Gelb, B. D. (2000). Mutations in TFAP2B cause Char syndrome, a familial form of patent ductus arteriosus. *Nat. Genet.* **25**, 42-46.

Schott, J. J., Benson, D. W., Basson, C. T., Pease, W., Silberbach, G. M., Moak, J. P., Maron, B. J., Seidman, C. E. and Seidman, J. G. (1998). Congenital heart disease caused by mutations in the transcription factor NKX2.5. *Science* **281**, 108-111.

Schuffenhauer, S., Lichtner, P., Peykar-Derakhshandeh, P., Murken, J., Haas, O. A., Back, E., Wolff, G., Zabel, B., Barisic, I., Rauch, A. et al. (1998). Deletion mapping on chromosome 10p and definition of a critical region for the second DiGeorge syndrome locus (DGS2). *Eur. J. Hum. Genet*. **6**, 213-225.

Srinivaswan, S., Scott, B. H., Aristizabal, O., Lia, K., Labow, M., Artman, M. and Turnbull, D. (1998). Noninvasive in utero imaging of mouse embryonic heart development with 40-MHz echocardiography. *Circulation* **98**, 912-918.

Strauss, A. (1998). The molecular basis of congenital cardiac disease. *Semin. Thoracic Cardiovasc. Surg.* **1**, 179-188.

Svenson, K., Bogue, M. and Peters, L. (2003). Identifying new mouse models of cardiovascular disease: a review of high throughput screens of mutagenized and inbred strains. *J. Appl. Physiol.* **94**, 1650-1659.

Tamagnone, L. and Comoglio, P. M. (2004). To move or not to move? *EMBO Rep.* **5**, 356-361.

Tartaglia, M., Mehler, E. L., Goldberg, R., Zampino, G., Brunner, H. G., Kremer, H., van der Burgt, I., Crosby, A. H., Ion, A., Jeffery, S. et al. (2001). Mutations in PTPN11 encoding for protein tyhrosine phosphatase SHP-2, cause Noonan syndrome. *Nat. Genet.* **29**, 465-468.

Toyofuku, T., Yabuki, M., Otsu, K., Kuzuya, T., Hori, M. and Tada, M. (1998). Direct association of the gap junction protein connexin-43 with ZO-1 in cardiac myocytes. *J. Biol. Chem.* **273**, 12725-12731.

Van Esch, H., Groenen, P., Fryns, J., van de Ven, W. and Devriendt, K. (1999). The phenotypic spectrum of the 10p deletion syndrome versus the classical DiGeorge syndrome. *Genet. Couns.* **10**, 59-65.

Vitaterna, M., King, D.-P., Chang, A., Kornhauser, J., Lowrey, P., McDonald, J., Dove, W., Pinto, L., Truek, F. and Takahashi, J. (1994). Mutagenesis and mapping of a mouse gene, Clock, essential for circadian behavior. *Science* **264**, 719-725.

Weber, J., Salinger, A. and Justice, M. (2000). Optimal N-ethyl-N-nitrosourea (ENU) doses for inbred mouse strains. *Genesis* **26**, 230-233.

Weninger, W. J. and Mohun, T. (2002). Phenotyping transgenic embryos: a rapid 3-D screening method based on episcopic fluorescence image capturing. *Nat. Genet.* **30**, 59-65.

Yagi, H., Furutani, Y., Hamada, H., Sasaki, T., Asakawa, S., Mionoshima, S., Ichida, F., Joo, K., Kimura, M., Imamura, S. et al. (2003). Role of Tbx1 in human del22q11.2 syndrome. *Lancet* **362**, 1366-1373.

Yamagishi, C., Heirck, B., Gittenberger-de Groot, A., Yamagishi, H. and Srivastava, D. (2003). Functional attenuation of UFD1l, a 22q11.2 deletion syndrome candidate gene, leads to cardiac outflow septation defects in chicken embryos. *Pediatr. Res.* **53**, 546-553

Zhou, Y., Foster, F., Qu, D., Zhang, M., Harasiewicz, K. and Adamson, S. (2002). Applications for multifrequency ultrasound biomicroscopy in mice from implantation to adulthood. *Physiol. Genomics* **10**, 1-14.